Linear–electric-field effect on g values of low-symmetry cupric sites

Bernard S. Gerstman
Department of Physics, Florida International University, Miami, Florida 33199
and Department of Physics, University of Virginia, Charlottesville, Virginia 22901

Arthur S. Brill
Department of Physics, University of Virginia, Charlottesville, Virginia 22901
(Received 21 August 1987)

We have investigated the linear–electric-field effect (LEFE) in cupric ions situated in ligand fields of low symmetry. General properties of LEFE signals resulting from various low-symmetry models are described. Treating g values, we show how hybrid-orbital "united-atom" models can be used for direct calculation of the LEFE signal expected from cupric sites of specific low-symmetry geometries. This hybrid–atomic-orbital approach is shown to give a straightforward method for interpreting LEFE data in terms of cupric electronic states that directly reflect the ligand environment. Results are presented which demonstrate the potential of calculations with this model to account quantitatively for the LEFE data from blue cupric proteins.

I. INTRODUCTION

Our investigations of the cupric ion in the protein azurin have led us to consider the linear–electric-field effect in low-symmetry cupric complexes in general. Upon application of an electric field some substances exhibit changes in their EPR signal. This is known as the linear–electric-field effect (LEFE). A variety of data from copper-containing blue cupric proteins [absorption, circular dichroism (CD), EPR, and MCD] have been successfully explained with a hybrid atomic orbital model. We have now used this approach to investigate the LEFE of similar low-symmetry cupric sites, treating g values in this paper. The hybrid–atomic-orbital model (HAOM) model is used to show how LEFE data can be interpreted in terms of cupric electronic states that directly reflect the ligand environment. Further, modeling of the LEFE involves matrix elements that appear in calculations of other observables already investigated, but in new combinations. Thus new and significant constraints may be placed upon a model by inclusion of the LEFE behavior.

The LEFE in electron paramagnetic resonance (EPR) was observed in 1961 (Ref. 1) in inorganic systems. Bloembergen[2] specifically pointed out that an LEFE signal, which is linear with the strength of the applied electric field E_{applied} is only possible for a paramagnetic ion located in an environment that does not have inversion symmetry. Mims[3] used a spin Hamiltonian tensor formalism to formulate the problem and Kiel[4] and Kiel and Mims[5] described the LEFE for various rare-earth ions in $CaWO_4$ using an "equivalent even interaction" between states. Bates[6] employed crystal field theory and a hybrid–atomic-orbital model for theoretical discussion of the linear–electric-field effect for cupric ions residing in tetragonally and trigonally distorted tetrahedral fields. It is this approach that we follow and expand upon to investigate the LEFE of cupric ions in low-symmetry environments. Roitsin[7] wrote an excellent review in 1971 of the work done on LEFE up to that time and Mims[8] later wrote a valuable book on the LEFE.

The LEFE has also been used to investigate metal sites in proteins. Peisach and Mims[9] measured the LEFE in cytochrome P-450 in order to characterize the ligand arrangement around the ferric ion. Mims and Peisach[10,11] also made measurements on a variety of ferric heme systems to determine the crystal field environment and ligand binding of the iron.

More recently, Peisach and Mims[12] have taken LEFE measurements on the proteins azurin and stellacyanin. These proteins are known as blue cupric proteins[13,14] because of strong light absorption by the metal site due to the environment supplied by the enfolding protein shell. LEFE measurements are sensitive to deviations from centrosymmetry of the cupric ion's environment and therefore can be a valuable source of information on the electronic structure of the cupric ion.

Our interest is in how the environment of a metal ion influences its electronic states. Calculations of spectroscopic and functional properties of the metal are facilitated if the arrangement of the surrounding ligands contains symmetry operations. The higher the point group, the more degeneracies exist and this leads to fewer independent matrix elements to calculate. In low-symmetry complexes such as in proteins, the metal ion's ligand configuration contains few symmetry operations and may in fact belong to the lowest-symmetry point group, C_1, which contains only the identity operation. To facilitate calculations, the system under study can be approximated as having a ligand arrangement consistent with a geometrically appropriate group of higher symmetry. We have used this approach in the past in studying various spectroscopic properties of low-symmetry sites.[15–18]

However, the actual departures from true symmetry can be important in explaining spectroscopic and func-

tional properties of the molecule. In this paper we show how LEFE measurements can be used as a quantitative guide, limited by the uncertainty in the local electric field, in modifying the electronic states of an HAOM describing a cupric site in order to reflect the departures from the higher-symmetry group.

II. LEFE

A. Polycrystalline, powder, and frozen solution samples

Experimentally, the LEFE manifests itself as a shift in the EPR resonance frequency of a paramagnetic center upon application of a dc electric field. Since the electric field has odd parity under spatial inversion, a linear effect will only be observed for a paramagnetic center located in an environment that does not have inversion symmetry (noncentrosymmetric). This, in fact, gives the LEFE especial value because observation of measurable effects with other EPR techniques (that do not include an applied electric field) does not require the existence of noncentrosymmetric components of the ligand field.

The simplest technique to measure the LEFE is to apply a dc electric field to the sample in a standard EPR experiment and measure the change in the resonance frequency directly. This approach can be used in samples where the LEFE is large enough to shift the lines by an amount greater than their width. However, problems can arise in the application of this simple method. The sample may not be capable of withstanding large applied electric fields, or the size of the LEFE may be too small relative to the linewidth to be observable. In these situations, the electron-spin-echo method, which is limited by the width of individual spin packets rather than the width of the overall line, is valuable.

EPR experiments on proteins are often done on frozen solutions. In this case, the EPR absorption extends between limits determined by (apart from hyperfine separations) the maximum and minimum values of g. For azurin at 9.2 GHz, this extent is several hundred gauss, with first derivative "lines" having full width at half-height of no less than 30 G. As will be seen below, for laboratory fields across the sample of 10^5 V/cm, an LEFE of the order of 1 G is expected. This makes the direct method useless. On the other hand, the width of individual spin packets may be only 0.1 G in biological materials (Ref. 8, p. 238) which is small enough to allow the spin-echo technique to be used profitably. The spin-echo method for LEFE measurements has been described in detail elsewhere.[8,19]

B. Notation for comparison of calculations with experimental data

As with any investigation, the choice of parameters that act as a bridge to connect theoretical descriptions with experimental measurements is important for clarity. Mims[20] has developed a notation using a spin Hamiltonian tensor formalism. We base our description upon this and Mims and Peisach's work.[11] The parameter connecting experiment and theory is σ. Experimentally it is

$$\sigma = 2\pi/6\omega(E_{\text{applied}}\tau)_{1/2} , \tag{1}$$

where ω is the microwave angular frequency, and $(E_{\text{applied}}\tau)_{1/2}$ is the product of applied electric field E_{applied} and time τ between microwave pulses that produces a 50% reduction in the echo amplitude compared to the case of no applied **E** field. The time at which this occurs, $\tau_{1/2}$, gives the shift in the resonant frequency, $\delta\omega$ (Ref. 8),

$$\delta\omega = \frac{2\pi}{6\tau_{1/2}} . \tag{2}$$

This enables us to write Eq. (1) as

$$\sigma = (\delta\omega/\omega)/E_{\text{applied}} . \tag{3}$$

For any spin packet, in the absence of hyperfine effects, $\delta\omega/\omega = \delta g/g$. In a polycrystalline or frozen solution sample there will be a distribution in shifts and therefore the general expression relating σ to δg is

$$\sigma = K(\delta g/g)/E_{\text{applied}} . \tag{4}$$

The factor K is determined by the distribution of $\delta\omega$ at a given magnetic field setting, $\mathbf{B}_0$. This distribution arises because at any magnetic field setting similar paramagnetic centers can have the same g value but be oriented over a range of angles, θ,ϕ, where the g value is given as

$$g(\theta,\phi) = (g_3^2\cos^2\theta + g_2^2\sin^2\theta\sin^2\phi + g_1^2\sin^2\theta\cos^2\phi)^{1/2} . \tag{5}$$

In Eq. (5) $g_3 = g_z = g_{\max}$, $g_2 = g_y$, and $g_1 = g_x = g_{\min}$. (In assigning the number subscripted g's in this way, we follow the LEFE literature. In another convention g_1 and g_3 correspond to the lowest and highest field resonances, respectively.) Since each principal value of the g tensor, g_1, g_2, g_3, may have a different δg, the observed $\delta\omega$ is a weighted average of the contributing δg's. The weighting distribution (see Refs. 8, 11, and 19) varies with the field setting $\mathbf{B}_0$, and therefore so will K, although at all field settings $K \simeq 1$. In this paper we will focus our analysis on the LEFE at the two endpoints of the spectrum where analytical expressions linking frequency shifts with δg's can be derived. Further, we will show that the endpoints are the most valuable parts of the LEFE spectrum for supplying new information about the symmetry-lowering deviations in the ligand environment of low-symmetry cupric sites.

C. C_{ij} coefficients and dependence upon field setting

We use a set of coefficients, C_{ij}, to describe the electric field induced shifts:

$$C_{ij} = \frac{dg_j}{dE_i} , \tag{6}$$

where the g_j are the principal values of the diagonalized g tensor and **E** is the local electric field. This is similar to the description of Mims and Peisach[11] who use B_{ij} coefficients. If a diagonal g^2 tensor is used, the C_{ij} coefficients are related to the B_{ij} coefficients by

$$B_{ij}=2g_j\frac{dg_j}{dE_i}=2g_jC_{ij}\ . \tag{7}$$

We use the C_{ij} because they are a simpler description at the endpoints of the spectrum upon which we concentrate in this paper.

A complete description of the LEFE requires the full g tensor

$$\begin{bmatrix} g_{11} & g_{12} & g_{13} \\ g_{21} & g_{22} & g_{23} \\ g_{31} & g_{32} & g_{33} \end{bmatrix} = \begin{bmatrix} g_1 & g_6 & g_5 \\ g_6 & g_2 & g_4 \\ g_5 & g_4 & g_3 \end{bmatrix} . \tag{8}$$

The g tensor is shown with normal matrix notation as well as modified Voight notation where the principal values are listed as g_1, g_2, and g_3. If one uses the standard matrix notation for the g tensor, i.e., the left matrix in (8), then the C coefficients of Eq. (6) would actually require three subscripts representing the three degrees of freedom for the LEFE

$$C_{ijk}=\frac{dg_{jk}}{dE_i}\ . \tag{6'}$$

We will use the modified Voight notation which suppresses one of the subscripts. A paramagnetic center which has a symmetric g tensor in the absence of an applied electric field does not necessarily have a symmetric g tensor upon application of an electric field which causes $g_{ij}\rightarrow g_{ij}+\delta g_{ij}$. However, if one is concerned only with the endpoints, then only principal values of the g tensor are involved and whether or not the tensor is symmetric is unimportant.

With six independent elements of the g tensor and three possible directions of the applied electric field, there are an unwieldy 18 independent LEFE coefficients C_{ij} of Eq. (6), where $j=1-6$ from matrix (8), and $i=1,2,3$ corresponding to x,y,z, respectively. At EPR magnetic field settings, $\mathbf{B}_0$, in the middle of the spectrum, all 18 coefficients may contribute to the observed LEFE since the distribution in paramagnetic center orientation allows contributions from all elements of the g tensor. By focusing on the endpoints of the EPR (and LEFE) spectrum, we greatly reduce the number of contributing C_{ij}.

D. LEFE and C_{ij} at endpoints

The low-field endpoint corresponds to only those paramagnetic centers oriented such that the principal axis of the largest g value ($g_3=g_z$) is aligned along the direction of the magnetic field $\mathbf{B}_0$, and analogously for the high field endpoint and g_1. All molecules contributing to the extreme low-field EPR signals will be oriented with their molecular z axis parallel or antiparallel to $\mathbf{B}_0$, and will have the same $|\delta\omega|\propto|\delta g_3|$ (apart from possible small differences in the environment of the paramagnetic center from molecule to molecule). At the high-field end, $|\delta\omega|\propto|\delta g_1|$. There are still three possible contributing C_{ij} at the low-field endpoint, and another three at the high-field endpoint, because $\mathbf{E}_{\text{applied}}$ can be applied in the x, y, or z directions. Indeed, the orientation of $\mathbf{E}_{\text{applied}}$ is completely independent of $\mathbf{B}_0$. However, the information available from studies of frozen protein solutions is fully obtained with $\mathbf{E}_{\text{applied}}$ either parallel or perpendicular to $\mathbf{B}_0$. (Measurements made at intermediate orientations reflect a convolution of the data obtained at $E_{\text{applied}}\|\mathbf{B}_0$ and $\mathbf{E}_{\text{applied}}\perp\mathbf{B}_0$.[8,11]) Thus two values of the σ of Eq. (3) are measured at each endpoint, with the notation $\sigma_{\|,3}$ for $\mathbf{E}_{\text{applied}}\|\mathbf{B}_0$ and $\sigma_{\perp,3}$ for $\mathbf{E}_{\text{applied}}\perp\mathbf{B}_0$ at the low-field endpoint, and likewise for g_1 at the high-field endpoint.

We take the local field $\mathbf{E}_L$ to be linearly related to the applied field,

$$\mathbf{E}_L=\mathbf{E}=R\,\mathbf{E}_{\text{applied}}\ . \tag{9}$$

For $\sigma_{\|,3}$, $E_z=RE_{\text{applied}}$ and $E_x=E_y=0$. With no distribution in shifts at the field extrema, Eq. (4) is applicable with $K=1$ and, with Eqs. (6) and (9), gives

$$\sigma_{\|,3}=RC_{33}/g_3\ . \tag{10}$$

$\sigma_{\perp,3}$, with $\mathbf{E}$ randomly distributed in the molecular x-y plane ($E_z=0$), has contributions from both $C_{13}=dg_z/dE_x$ and $C_{23}=dg_z/dE_y$. For this random distribution in the x-y plane, the spin-echo half fall parameter $(E_{\text{applied}}\tau)_{1/2}$ of Eq. (1) gives[8,11]

$$\sigma_{\perp,3}=R\,(C_{13}^2+C_{23}^2)^{1/2}/1.45g_3\ . \tag{11}$$

Similarly, at the high-field end one finds

$$\sigma_{\|,1}=RC_{11}/g_1$$

and

$$\sigma_{\perp,1}=R\,(C_{21}^2+C_{31}^2)^{1/2}/1.45g_1\ . \tag{12}$$

Formulas (11) and (12) show that C_{ij} and C_{kj} are combined in quadrature and therefore their calculated signs are unimportant.

We now review the hybrid-atomic-orbital model which we use to describe the electronic states of low-symmetry cupric sites, and then show how the electronic states of the HAOM are used for calculating the C_{ij} coefficients. This formulation leads to a direct analysis of LEFE data in terms of HAOM states, states which are determined by the ligand environment of the paramagnetic ion.

III. HYBRID-ATOMIC-ORBITAL MODEL OF CUPRIC ELECTRONIC STATES

The higher the point group that a ligand environment belongs to, the more degeneracies exist, and the fewer matrix elements between electronic states of the central metal ion are required in calculating observables. With this in mind, we first describe the electronic structure of the cupric ion in blue proteins in terms of a ligand environment of D_2 point-group symmetry. D_2 symmetry is taken at the start for two reasons. Under D_2 symmetry the electronic states will transform as irreducible representations that obey selection rules that simplify calculations. Additionally, this symmetry is low enough for the electronic states to approximate those of the metal ion in its protein site which, in actuality, has an environment

with deviations from any symmetry group above C_1. Previous calculations have indeed shown that approximating the cupric site in azurin as having D_2 symmetry is useful for describing various experimental properties, the unusual hyperfine splitting being an interesting exception.[15,16,17,18] We demonstrate below how one can calculate LEFE parameters with a hybrid–atomic-orbital model, and also that the LEFE data on azurin cannot be explained with a site of D_2 symmetry. Clearly then, the LEFE data provide a basis for modifying the HAOM of D_2 symmetry used successfully for simulating other experimental phenomena and, thereby, making the model closer to the true electronic structure.

In the united atom HAOM the ligand parts of a delocalized state are taken as orbitals with the same angular dependences as the atomic orbitals of the central metal ion located in the ligand crystal field. Though centered on the metal ion, the radial functions of the ligand orbitals differ from those of the ion. With the symmetry of the site approximated as D_2, the ion and ligand orbitals can be assigned to irreducible representations (irreps) of the point group D_2. A ligand orbital will combine with a cupric orbital of the same irrep to form a hybrid-atomic orbital. This allows cupric $3d$ orbitals to mix with ligand orbitals that transform as cupric $4p$ orbitals but have extended radial functions. In a free cupric ion, the $4p$ orbitals would be too high in energy to mix appreciably with the $3d$ orbitals. The mixing is now stronger because the $4p$ orbitals are not pure metal orbitals but instead have a ligand contribution which forms two orbitals, one higher and one lower in energy than the pure cupric $4p$ orbital. The radially extended $4p$ orbital with lower energy can now mix with a cupric $3d$ orbital of the same symmetry. Similarly, mixing of $4s$ and $3d$ orbitals is also considered.

Eight hybrid-atomic orbitals result from the cupric $3d$ and extended $4p$ orbitals. The $4s$ orbitals are allowed to mix into the hybrid orbitals belonging to the A_1 irrep in the D_2 group. The cupric ion has a $3d^9$ configuration outside of closed shells and it is therefore convenient to view the outer shell as a single hole. This requires the ordering of the HAOM to be inverted and leads to Table I, reprinted from Fig. 3 of Ref. 18, for the ordering of the electronic states of the cupric $3d$ hole. Additional discussion of the states of Table I can be found in Refs. 16 and 18. We now develop an expression for the LEFE C_{ij} involving matrix elements between the electronic states of the cupric ion.

IV. THEORETICAL EXPRESSION FOR C_{ij}

A. Spin-orbit coupling and LEFE

Our calculation of the C_{ij} is an extension of the standard method for calculating g values

$$g \equiv \frac{1}{\mu_B}\frac{d(\Delta E)}{dB} , \tag{13}$$

where ΔE is the energy splitting between the members of a Kramers doublet arising from a ground-state orbital singlet upon application of an external magnetic field, $\mathbf{B}$. μ_B is the Bohr magneton. In EPR experiments one is usually interested in energy splittings that are first order in the applied field and ΔE can be expressed as

$$\frac{\Delta E}{2} = \frac{g}{2}\mu_B B = \langle 1\alpha_1 | \mathcal{H}' | 1\alpha_1 \rangle = -\langle 1\alpha_2 | \mathcal{H}' | 1\alpha_2 \rangle . \tag{14}$$

The states $|1\alpha_1\rangle$ and $|1\alpha_2\rangle$ represent the two members of the ground-state Kramers doublet. $\mathcal{H}'$ is the Hamiltonian representing the perturbation of the applied magnetic field

$$\mathcal{H}' = \boldsymbol{\mu}\cdot\mathbf{B} = \mu_{z_l} B = -\mu_B (L_{z_l} + 2S_{z_l}) B , \tag{15}$$

where the applied field $\mathbf{B}$ is applied along the laboratory z_l axis. For the low-field (g_3) resonance, the molecular z and laboratory z_l directions are parallel.

If spin-orbit coupling between the ground spin doublet and excited states is neglected, $|1\alpha_1\rangle$ and $|1\alpha_2\rangle$ can each be written as a product of the ground-state orbital singlet times a pure spin state; $|1\alpha_1\rangle = |1\rangle|+\rangle$ and $|1\alpha_2\rangle = |1\rangle|-\rangle$. $|1\rangle$ represents the orbital ground-state singlet and $|+\rangle, |-\rangle$ are the two possible spin substates defined by their projections along the laboratory z_l axis. With an orbital singlet resulting from the

TABLE I. Hybrid–atomic-orbital model energy-level diagram for the single cupric hole in which all states transform as irreducible representations of the D_2 point group.

$$|B_3'\rangle = (1-\beta_3^2)^{1/2}|3d_{yz}\rangle - \beta_3|4p_x\rangle$$

$$|B_2'\rangle = (1-\beta_2^2)^{1/2}|3d_{xz}\rangle - \beta_2|4p_y\rangle$$

$$|B_1'\rangle = (1-\beta_1^2)^{1/2}|3d_{xy}\rangle - \beta_1|4p_z\rangle$$

$$|B_3\rangle = \beta_3|3d_{yz}\rangle + (1-\beta_3^2)^{1/2}|4p_x\rangle$$

$$|B_2\rangle = \beta_2|3d_{xz}\rangle + (1-\beta_2^2)^{1/2}|4p_y\rangle$$

$$|A_1'\rangle = \frac{1}{[(1+\gamma^2)(1+\delta^2)]^{1/2}}(|3d_{x^2-y^2}\rangle + \gamma|4s\rangle) - \frac{\delta}{(1+\delta^2)^{1/2}}|3d_{z^2}\rangle$$

$$|A_1\rangle = \frac{1}{(1+\delta^2)^{1/2}}|3d_{z^2}\rangle + \frac{1}{[(1+\gamma^2)(1+\delta^2)]^{1/2}}(\delta|3d_{x^2-y^2}\rangle + \gamma\delta|4s\rangle)$$

$$|B_1\rangle = \beta_1|3d_{xy}\rangle + (1-\beta_1^2)^{1/2}|4p_z\rangle$$

ligand field, angular momentum is quenched; the only contribution to the energy splitting [Eqs. (13) and (14)] in a magnetic field is from the spin of the states, and g has the free hole (electron) value of 2.0023 which we shall approximate as 2.00.

If spin-orbit coupling is included, various excited-state orbital-spin combinations are mixed into the ground-state Kramers doublet; $|1\alpha_1\rangle$ and $|1\alpha_2\rangle$ are now generally each composed of several orbital-spin combinations rather than just a single product. Equation (14) remains valid to first order in **B**, but now the g value of the ground state may differ significantly from the free electron value and be anisotropic, as shown in Eq. (5).

There are two equivalent ways of using Eq. (14) for calculating the g value in the presence of spin-orbit coupling. One method is to use the Hamiltonian of Eq. (15) and take matrix elements between states that have been corrected for spin-orbit coupling. The perturbation is treated to first order but the ground state $|1\alpha_1\rangle$ includes, in addition to $|1\rangle|+\rangle$, a linear combination of excited orbital-spin states; likewise, for $|1\alpha_2\rangle$. Alternatively, Eq. (14) can be used with the non-spin-orbit-corrected, ligand field-fashioned $|1\alpha_1\rangle=|1\rangle|+\rangle$ and $|1\alpha_2\rangle=|1\rangle|-\rangle$, but with a Hamiltonian different than that of Eq. (15). To take into account spin-orbit coupling, the perturbation Hamiltonian is modified to

$$\mathcal{H}'=\lambda\mathbf{L}\cdot\mathbf{S}+\mu_B(\mathbf{L}+2\mathbf{S})\cdot\mathbf{B} \tag{16}$$

and the non-spin-orbit-corrected ground states are treated to second order in $\mathcal{H}'$.

The two methods give identical results—a g value that differs, because of spin-orbit coupling, from the spin-only value of 2.00. The contribution of spin-orbit coupling to the g value depends on the complex. For example, in azurin, the cupric site has $g_1=2.04$ and $g_3=2.27$. The maximum spin-orbit contribution, $\Delta g_{\max}=g_{\max}-2.00=0.27$, is small relative to the spin-only contribution, but is of crucial importance to the LEFE. An externally applied electric field will cause a noticeable change only in the spin-orbit contribution to the overall g value. The effect of the applied electric field on the free spin part will be negligible. For this reason, the LEFE depends strongly on spin-orbit coupling within the HAOM. We later derive a rigorous expression for the C_{ij} which incorporates spin-orbit coupling explicitly. This allows the LEFE to be used to obtain information on the states of the HAOM as formed under the influence of the ligand environment.

B. Order-of-magnitude estimate of C_{ij}

It is instructive to compare the magnitudes of δg due to the applied electric field with the intrinsic Δg arising from spin-orbit coupling alone. The magnitude of Δg is, approximately,

$$\Delta g_{ii}\sim\frac{\langle 1|\lambda L_i|j\rangle\langle j|L_i|1\rangle}{E_1-E_j}\ ,$$

where $|1\rangle$, $|j\rangle$ are non-spin-orbit-corrected, ligand field states, and E_1, E_j are the ligand field-induced energies of the states (also uncorrected for the spin-orbit interaction). Likewise, the magnitude of δg due to the electric field E is

$$\delta g_{ii}\sim\frac{eE\langle 1|r|k\rangle\langle k|\lambda L_i|j\rangle\langle j|L_i|1\rangle}{(E_1-E_k)(E_1-E_j)}\ .$$

The relative sizes of the field-induced and intrinsic contributions to the g values are, therefore,

$$\frac{\delta g}{\Delta g}\sim\frac{eE\langle 1|r|k\rangle}{E_1-E_k}\ .$$

With $E\sim10^5$ V/cm, $\langle 1|r|k\rangle\sim1$ Å, and $E_k-E_1\sim10^4$ cm^{-1}, this ratio is $\delta g/\Delta g\sim10^{-3}$. With Δg already seen to be of order 10^{-1}, the magnitude of δg is 10^{-4}. This δg corresponds to a shift in resonance magnetic field strength of less than 1 G at 9.2 GHz. The size of the shift, far smaller than the widths of the resonances, necessitates the use of the spin-echo measurement technique.[19,20]

A δg of 10^{-4} expected from an applied field of 10^5 V/cm leads, from Eq. (6), to an estimate for the C_{ij}, and for the experimentally measured parameters $\sigma\sim C_{ij}/g$, of 10^{-9} cm/V.

C. Formulation of the C_{ij}

Equations (6), (13), and (14) will now be used to get a rigorous expression for the coefficients C_{ij}. As shown in Eq. (6'), the linear-electric-field-effect coefficients actually involve three indices. These three indices represent the three separate perturbations that cause an energy splitting of the ground-state Kramers doublet. The three perturbations are $\lambda\mathbf{L}\cdot\mathbf{S}$, $\boldsymbol{\mu}\cdot\mathbf{B}$, and $e\mathbf{E}\cdot\mathbf{r}$, corresponding to the spin-orbit interaction, an applied magnetic field, and an applied electric field, respectively. In the absence of these perturbations each member of the Kramers pair is a simple product of an HAOM orbital with a pure spin state and the two members of the pair are degenerate. These perturbations act in different manners to admix HAOM states and produce an energy splitting in the Kramers doublet.

From Eqs. (6), (13), and (14) we see that the LEFE C_{ij} coefficients depend upon the energy splitting of the ground-state Kramers doublet. To calculate the C_{ij} coefficients, we derive an expression for the third-order energy splitting of the HAOM Kramers pair and retain terms that are linear in λ, **B**, and **E** since these are the terms to which the LEFE is sensitive. The final expression for the C_{ij} will involve matrix elements between HAOM orbitals only. The value of this approach is that LEFE data can then be used as a direct probe of HAOM states and therefore of the ligand environment.

The perturbation Hamiltonian is of the form

$$\mathcal{H}'=\lambda\mathbf{L}\cdot\mathbf{S}+\mu_B\mathbf{B}\cdot(\mathbf{L}+2\mathbf{S})+e\mathbf{E}\cdot\mathbf{r}\ . \tag{17}$$

We now calculate the third-order correction to the energy of one member of the unperturbed ground-state Kramers pair using[21]

$$\Delta E_{1+}=\sum_{m\,(\neq 1)}\sum_{q\,(\neq 1)}\frac{\langle 1+|\mathcal{H}'|m\rangle\langle m|\mathcal{H}'|q\rangle\langle q|\mathcal{H}'|1+\rangle}{(E_m-E_1)(E_q-E_1)}-\sum_{m\,(\neq 1)}\frac{\langle 1+|\mathcal{H}'|1+\rangle\langle 1+|\mathcal{H}'|m\rangle\langle m|\mathcal{H}'|1+\rangle}{(E_m-E_1)^2}\,. \tag{18}$$

Bates[6] has taken a different approach in treating the states and the various perturbations. Our method has the value of immediately focusing directly on the HAOM states of interest. The following results incorporate all of Bates's expressions and include additional terms not included by Bates but which are important in considering cupric sites of lower symmetry than considered by Bates.

From Eq. (18) we retain terms linear in each of the three perturbations since these terms are the dominant contribution to the LEFE. (Higher-order terms in λ may also contribute, but will be orders of magnitude smaller in effect.) We leave out terms containing matrix elements of the form $\langle 1|\mathbf{L}|1\rangle$ because these are zero due to orbital angular momentum "quenching" of singlet orbital states resulting from a low-symmetry ligand field.[22] The expression for the energy shift of one member of the ground-state Kramers doublet is, exclusive of spin matrix elements,

$$\Delta E_1=2e\mu_B\left[\sum_{m\,(\neq 1)}\sum_{q\,(\neq 1)}(\langle 1|\mathbf{E}\cdot\mathbf{r}|m\rangle\langle m|\mathbf{B}\cdot\mathbf{L}|q\rangle\langle q|\lambda\mathbf{L}|1\rangle+\langle 1|\mathbf{E}\cdot\mathbf{r}|m\rangle\langle m|\lambda\mathbf{L}|q\rangle\langle q|\mathbf{B}\cdot\mathbf{L}|1\rangle+\langle 1|\mathbf{B}\cdot\mathbf{L}|m\rangle\langle m|\mathbf{E}\cdot\mathbf{r}|q\rangle\langle q|\lambda\mathbf{L}|1\rangle)/(E_m-E_1)(E_q-E_1)-\sum_{m\,(\neq 1)}\langle 1|\mathbf{E}\cdot\mathbf{r}|1\rangle\langle 1|\mathbf{B}\cdot\mathbf{L}|m\rangle\langle m|\lambda\mathbf{L}|1\rangle/(E_m-E_1)^2\right]. \tag{19}$$

For shifts in g that are linear in $\mathbf{B}$ and $\mathbf{E}$ we can use the standard expression

$$\delta g=\frac{2\Delta E_1}{\mu_B B}\,. \tag{20}$$

Equations (20) and (6′) give

$$C_{ijk}=\frac{\delta g_{jk}}{E_i}=\frac{2\Delta E_1}{E_i\mu_B B_j}\,. \tag{21}$$

The k subscript refers to the component of $\mathbf{L}$ from the spin-orbit interaction. Equations (19) and (21) give

$$C_{ijk}=4e\left[\sum_{m\,(\neq 1)}\sum_{q\,(\neq 1)}(\langle 1|r_i|m\rangle\langle m|L_j|q\rangle\langle q|\lambda L_k|1\rangle+\langle 1|r_i|m\rangle\langle m|\lambda L_k|q\rangle\langle q|L_j|1\rangle+\langle 1|L_j|m\rangle\langle m|r_i|q\rangle\langle q|\lambda L_k|1\rangle)/(E_m-E_1)(E_q-E_1)-\sum_{m\,(\neq 1)}\langle 1|r_i|1\rangle\langle 1|L_j|m\rangle\langle m|\lambda L_k|1\rangle/(E_m-E_1)^2\right]. \tag{22}$$

If one is interested only in the shift in the principal values of the g tensor, $j=k$ and Eq. (21) can be written with only two subscripts

$$C_{ij}=\frac{\delta g_j}{E_i}=\frac{2\,\Delta E_1}{E_i\mu_B B_j}\,. \tag{23}$$

In Eq. (23) it is understood that for principal values of the g tensor, $j=1-3$. We can now write the explicit expression for the C_{ij} for the principal values of the g tensor

$$C_{ij}=4e\left[\sum_{m\,(\neq 1)}\sum_{q\,(\neq 1)}(\langle 1|r_i|m\rangle\langle m|L_j|q\rangle\langle q|\lambda L_j|1\rangle+\langle 1|r_i|m\rangle\langle m|\lambda L_j|q\rangle\langle q|L_j|1\rangle+\langle 1|L_j|m\rangle\langle m|r_i|q\rangle\langle q|\lambda L_j|1\rangle)/(E_m-E_1)(E_q-E_1)-\sum_{m\,(\neq 1)}\frac{\langle 1|r_i|1\rangle\langle 1|L_j|m\rangle\langle m|\lambda L_j|1\rangle}{(E_m-E_1)^2}\right]. \tag{24}$$

Equation (24) will be used to calculate g-value contributions to experimental LEFE σ's in terms of states of the HAOM.

We note here an additional consideration. Equations (19)–(24) show that, in order to get the magnitude of δg, the calculated C_{ij} are to be multiplied by the local electric field actually experienced by the Cu ion, which may not be the same as the macroscopic applied field. This is why the right-hand side of Eqs. (10)–(12), connecting the calculated C_{ij} to the observed σ, is multiplied by the ratio of the local field to the applied field, $R = E_L / E_{\text{applied}}$. The greater this ratio, the smaller is the size of the calculated C_{ij} needed to simulate the observed σ. For inorganic crystals, this ratio is often taken[8] to be the Lorentz factor $(2+\epsilon)/3$, where ϵ is the dielectric constant of the crystal. However, for a sample of protein molecules frozen in ice, the analysis is more complicated because the cupric ion is imbedded in a protein shell surrounded by a phase with a different dielectric constant. Furthermore, there are sulfur atoms, of large polarizability, neighboring the cupric ion. We treat this situation in the Appendix and conclude that, in terms of the structural information available at the present time, one is limited to taking for R (a ratio which may well be significantly anisotropic) an average value equal to the Lorentz factor $(2+\epsilon)/3$, where ϵ is the dielectric constant of the surrounding phase.

V. C_{ij} FOR LOW-SYMMETRY SITES

A. D_2 symmetry and LEFE at endpoints

The point symmetry of the ligand environment enables one to determine by inspection which of the C_{ij} are nonzero, thus saving one the trouble of carrying out calculations that lead to zero values for coefficients. The nonzero components of the C_{ij} matrix ($\mathbf{C}$) can be identified for any point group by determining how the full matrix $\mathbf{C}$ transforms under a general transformation of the coordinate system represented by a 3×3 matrix with components which are the direction cosines of the new and old axes. Which of the components are nonzero is then arrived at by requiring the C_{ij} matrix to remain invariant under any symmetry operation allowed by the point group under consideration.

As an example, if the site is inverted through the origin, the transformed matrix $\mathbf{C}'$ is related to the original by $\mathbf{C}'=-\mathbf{C}$. If the point group of the site contains the inversion operator, then the transformed matrix $\mathbf{C}'$ must also obey $\mathbf{C}'=\mathbf{C}$. These two conditions require that $\mathbf{C}=0$, thus proving that there can be no LEFE in a site with inversion symmetry. With arguments of this type, all nonzero components of the 18 possible C_{ij} (C_{ijk}) can be identified. The nonzero entries for the LEFE are identical to those for the piezoelectric effect which is also described by a third-rank tensor. These nonzero components can be found in Ref. 23.

We now determine how LEFE data, especially at the endpoints, can be used to determine what modifications should be made to the states of an HAOM that were originally written as D_2 irreps (Table I). This will result in a truer model of the actual electronic states. These results are, of course, valid whether the molecular system is of biological origin or not.

The LEFE data on the cupric sites in azurin and stellacyanin (Figs. 7 and 8 of Ref. 12) show nonzero effects at the endpoints of the spectrum. From Eqs. (10), (11), and (12), endpoint signals require that some of the following coefficients be nonzero: C_{11} (C_{111}), C_{21} (C_{211}), C_{31} (C_{311}), C_{13} (C_{133}), C_{23} (C_{233}), C_{33} (C_{333}). From matrix (8), we see that these coefficients represent changes in principal values of the g tensor, and that in Eq. (22) the components of $\mathbf{L}$ and $\lambda\mathbf{L}$ must be the same, i.e., $j=k$, as shown in Eq. (24). However, for D_2 symmetry these coefficients will all be zero, as we now show.

A fundamental theorem of group theory (basis-function orthogonality theorem[24]) is that a matrix element $\langle j \mid \mathcal{H}' \mid k \rangle$ must be zero unless the direct product of the irreps of the states and the $\mathcal{H}'$ operator contains the totally symmetric or identical representation, Γ_1; i.e.,

$$\Gamma_j \times \Gamma_{\mathcal{H}'} \times \Gamma_k = a_1\Gamma_1 + \sum_{n>1} a_n \Gamma_n \ , \tag{25}$$

with $a_1 \neq 0$. The expression for C_{ijk} [Eq. (22)] is of the form

$$C_{ijk} \sim \langle 1 \mid r_i \mid m \rangle \langle m \mid L_j \mid q \rangle \langle q \mid L_k \mid 1 \rangle \ . \tag{26}$$

Each of these three matrix elements must obey Eq. (25) if the C_{ijk} is to be nonzero. For example, if the last matrix element is to be nonzero then the irreps must obey

$$\Gamma(q) \times \Gamma(L_k) \times \Gamma(1) = \Gamma_1 \ . \tag{27}$$

[Note: Γ_1 symbolizes the identical representation for the point group and is also denoted by A_1, whereas $\Gamma(1)$ symbolizes the specific irrep of the ground state.] We have simplified Eq. (27) by taking into account that all D_2 irreps are one dimensional. Equation (27) can be rewritten as

$$\Gamma(q) = \Gamma(L_k) \times \Gamma(1) \ . \tag{27a}$$

This restriction of $\Gamma(q)$ then sets a condition on the middle matrix element of Eq. (26)

$$\Gamma(m) \times \Gamma(L_j) \times \Gamma(q) = \Gamma(m) \times \Gamma(L_j) \times \Gamma(L_k) \times \Gamma(1) = \Gamma_1 \ . \tag{28}$$

Similarly, Eq. (28) restricts the possible $\Gamma(m)$. This then imposes a condition upon the first matrix element, as expressed in Eq. (29), which incorporates the irreps of all the operators of Eq. (26)

$$\Gamma(1) \times \Gamma(r_i) \times \Gamma(L_j) \times \Gamma(L_k) \times \Gamma(1) = \Gamma_1 \ . \tag{29}$$

As an irrep of D_2, $\Gamma(1)$, the irrep of whichever orbital is the ground state, obeys $\Gamma(1) \times \Gamma(1) = \Gamma_1$. This, and the Abelian nature of the D_2 group, leaves us with

$$\Gamma(r_i) \times \Gamma(L_j) \times \Gamma(L_k) = \Gamma_1 \ . \tag{30}$$

If the symmetry of the point group is D_2, Eq. (30) can only be fulfilled if i, j, and k are all different. This proves that D_2 symmetry requires that all of the coefficients that

involve changes in the principal values of the g value ($j=k$) must be zero. Therefore, a paramagnetic center located in an environment of rigorous D_2 symmetry will not exhibit an LEFE signal at the endpoints of the EPR spectrum.

B. Descent in symmetry

In order to explain LEFE signals at endpoints of the spectrum it is necessary to use HAOM states that belong to irreps of a point group with symmetry lower than D_2. Our approach in lowering the symmetry is to stay close to the HAOM D_2 model of Table I because of its success in explaining other data, and its ease of use. We therefore have attempted to simulate the LEFE data of the blue cupric proteins by modifying the states of Table I as little as possible. The modifications that lower the symmetry to C_1 are mixings of orbitals from one D_2 irrep into another. Once we determine the required mixings, we can then determine the properties of the ligand field that causes them and, perhaps, postulate the ligand environment responsible.

Our aim is to make the least change possible in the D_2 HAOM. The necessity for modifications in the D_2 model has been shown above to be the presence of nonzero LEFE signals at the endpoints of the EPR spectrum. In actuality, only the presence of nonzero LEFE signals at the low-field (g_3) end requires modification of the D_2 model. The shape of the nonzero signal at the high-field end makes this part of the spectrum explainable in terms of the effects of the nuclear hyperfine interaction within the framework of the D_2 HAOM.

The hyperfine interaction can combine with the g value to change the resonance frequency. An upturn at the high-field end of the spectrum will result when the principal components of the hyperfine coupling tensor, **A**, obey $A_1 \ll A_2$ and/or A_3.[25] When this is true, molecules with their g_1 axis making a small angle with the applied magnetic field will contribute to the high-field EPR signal. This can produce an upswing in the high-field end of the LEFE signal even when the site has rigorous D_2 symmetry and could explain the high-field LEFE data for azurin and, possibly, stellacyanin.

The low-field data do require a lowering of some of the HAOM orbitals from D_2 symmetry. The following general results for the low-field end can be easily adapted to situations where the high-field data also require changes in the D_2 HAOM states. The arguments would be analogous only with $z \rightarrow x$ (or y) and $g_3 \rightarrow g_1$.

The LEFE data show that the predominant signal at the low-field end is $\sigma_{\perp,3}$. Equation (11) shows that this requires either or both of C_{13} and C_{23} to be nonzero. The second subscript 3 means that we are looking at the g_3 endpoint, and the other subscript shows that the changes in g_3 occur upon application of an external **E** field in the molecules' local x or y axes. Thus, our modifications in the states of the HAOM of Table I must allow an electric field in the molecular x or y direction to couple to a state(s) that will produce a change in g_3. Equations (14) and (16) show that the states that are involved in calculating g_3 are the ground state, and excited states that couple to the ground state via L_z, which are the $|A_1\rangle$ states. (If we were interested in changes in g_2 we would focus on the $|B_3\rangle$ state, and likewise changes in g_1 would involve the $|B_2\rangle$ state.) First we will investigate changes in the ground state that would lead to nonzero calculated C_{i3}.

C. Ground-state modifications to produce C_{i3}

Group theory allows immediate determination of the symmetry properties that admixtures to the ground state of Table I must have if they are to produce nonzero C_{13} or C_{23}. We will be lowering the symmetry of the HAOM by admixing into the ground state an orbital that does not transform as the D_2 irrep (B_1) of the ground state of Table I. However, we can still make use of selection rules if we describe components of operators and components of orbitals by their D_2 irreps. This is possible because each of the Cartesian x, y, or z components of the operators belongs to a different irrep. Table II(a) lists the D_2 irreps (in three notations) and the components of the operators and orbitals that transform as each irrep.

The ground state of Table I transforms as the Γ_z irrep because it is composed of $|d_{xy}\rangle$ and $|p_z\rangle$. After mixing in another orbital, we can still use D_2 selection rules if we take into account that the ground state is now a combination of more than one D_2 irrep. For example, after adding $|p_x\rangle$, the ground state can be described as $\Gamma_z+\Gamma_x$.

We now treat the last term in Eq. (24) for the C_{ij}; the analysis applies as well to the other terms. The direct products of irreps given in Table II(b) are used to determine which orbital must be added to the ground state to get a nonzero C_{13} ($i=1, j=3$).

$$C_{13} \sim \langle 1 | x | 1 \rangle \langle 1 | L_z | m \rangle \langle m | L_z | 1 \rangle \ . \tag{31}$$

The last two matrix elements of (31) are nonzero within the D_2 model of Table I if $|m\rangle$ is a state that transforms as an A_1 irrep. Therefore our new admixture need only make the first matrix element nonzero. This requires

$$\Gamma(1) \times \Gamma(x) \times \Gamma(1) \sim \Gamma_1 \ . \tag{32}$$

TABLE II. Information about the point group D_2. (a) Irreducible representations (three different notations) and components of orbitals and operators that transform as each. (b) Multiplication table for D_2 irreps (the group is Abelian).

Irreducible representation			Operators and orbitals
	(a)		
A_1	Γ_1		$d_{x^2-y^2}, d_{z^2}, 4s$
B_1	Γ_2	Γ_z	z, L_z; d_{xy}, p_z
B_2	Γ_3	Γ_y	y, L_y; d_{xz}, p_y
B_3	Γ_4	Γ_x	x, L_x; d_{yz}, p_x
	(b)		
$\Gamma_1 \times \Gamma_1 = \Gamma_1$			$\Gamma_2 \times \Gamma_2 = \Gamma_1$
$\Gamma_1 \times \Gamma_2 = \Gamma_2$			$\Gamma_2 \times \Gamma_3 = \Gamma_4$
$\Gamma_1 \times \Gamma_3 = \Gamma_3$			$\Gamma_2 \times \Gamma_4 = \Gamma_3$
$\Gamma_1 \times \Gamma_4 = \Gamma_4$			
$\Gamma_3 \times \Gamma_3 = \Gamma_1$			$\Gamma_4 \times \Gamma_4 = \Gamma_1$
$\Gamma_3 \times \Gamma_4 = \Gamma_2$			

TABLE III. Low-field endpoint LEFE coefficients for various energies and values of the hybridization coefficients of Fig. 2. $\delta = 1.0$.

	Energies (kcm^{-1})							Hybridization parameters										C_{13}	C_{23}	C_{33}	$C_{1,3}$
Case	A_1	A_1'	B_2	B_3	B_1'	B_2'	B_3'	β_1	β_2	β_3	γ	σ	b_{1x}	b_{1y}	a_{1x}	a_{1y}	b_{is}	($\times 10^{-5}$ Å/cm^{-1})			
A1a	7	10	13	16	25	22	19	0.85	0.80	0.80	0	0	0	0	0	0	0	0	0	0	0
A1b													0.10					0	0.76	0	0.54
A1c													0	0.10				0.75	0	0	0.53
A1d													0.10	0.10				0.74	0.75	0	0.75
B1a	7	15	11	12.5	17	21	19.5	0.94	0.94	0.94			0	0				0	0	0	0
B1b													0.10					0	0.99	0	0.70
B1c													0	0.10				0.99	0	0	0.70
B1d													0.10	0.10				0.97	0.97	0	0.97
A2a	7	10	13	16	25	22	19	0.85	0.80	0.80			0	0	0.10			−0.63	0	0	0.45
A2b															0	0.10		0	0.63	0	0.45
A2c															0.10	0.10		−0.62	0.62	0	0.62
B2a	7	15	11	12.5	17	21	19.5	0.94	0.94	0.94					0.10	0		−0.61	0	0	0.43
B2b															0	0.10		0	0.61	0	0.43
B2c															0.10	0.10		−0.61	0.61	0	0.61
A3a	7	10	13	16	25	22	19	0.85	0.80	0.80		0.25	0.10	0.10	0	0	−0.24	0.53	0.52	−1.47	0.53
A3b													0.20	0.20			−0.48	0.98	0.97	−1.28	0.98
B3a	7	15	11	12.5	17	21	19.5	0.94	0.94	0.94			0.10	0.10			−0.14	0.63	0.62	−1.12	0.63
B3b													0.20	0.20			−0.27	1.13	1.12	−1.01	1.13
B3c													0.30	0.30			−0.41	1.43	1.42	−0.87	1.43
A4a	7	10	13	16	25	22	19	0.85	0.80	0.80		0.15	0.10	0.10			−0.40	0.65	0.64	−0.94	0.65
A4b												0.20					−0.30	0.59	0.58	−1.22	0.59
B4a	7	15	11	12.5	17	21	19.5	0.94	0.94	0.94		0.15					−0.23	0.77	0.77	−0.69	0.77
B4b												0.20					−0.17	0.70	0.70	−0.89	0.70
B4c													0.20	0.20			−0.34	1.25	1.24	−0.84	1.25
A5a	7	10	13	16	25	22	19	0.85	0.80	0.80	0.20	0	0	0	0.05	0.05	−0.15	−0.23	0.35	0	0.30
A5b															0.10	0.10	−0.30	−0.46	0.69	0	0.59
A5c															0.15	0.15	−0.45	−0.68	1.02	0	0.87
B5a	7	15	11	12.5	17	21	19.5	0.94	0.94	0.94					0.10	0.10	−0.17	−0.45	0.67	0	0.57
B5b															0.15	0.15	−0.26	−0.67	1.00	0	0.85
B5c															0.20	0.20	−0.34	−0.86	1.28	0	1.09
A6a	7	10	13	16	25	22	19	0.85	0.80	0.80	0.50	0	0	0	0.10	0.10	−0.12	−0.20	0.60	0	0.45
A6b															0.20	0.20	−0.24	−0.39	1.15	0	0.86
B6a	7	15	11	12.5	17	21	19.5	0.94	0.94	0.94					0.10	0.10	−0.07	−0.20	0.58	0	0.43
B6b															0.20	0.20	−0.14	−0.38	1.12	0	0.84
B6c															0.40	0.40	−0.27	−0.65	1.92	0	1.43

TABLE IV. States directly involved in producing C_{13} and C_{23}.

$$|B_3\rangle = N_{B_3}^{-1}[\beta_3 |3d_{yz}\rangle + (1-\beta_3^2)^{1/2} |4p_x\rangle + b_{3s} |4s\rangle]$$

$$|B_2\rangle = N_{B_2}^{-1}[\beta_2 |3d_{xz}\rangle + (1-\beta_2^2)^{1/2} |4p_y\rangle + b_{2s} |4s\rangle]$$

$$|A_1\rangle = N_{A_1}^{-1}[(1+\gamma^2)^{1/2} |3d_{z^2}\rangle + \delta |3d_{x^2-y^2}\rangle + \gamma\delta |4s\rangle + a_{1x} |4p_x\rangle + a_{1y} |4p_y\rangle]$$

$$|B_1\rangle = N_{B_1}^{-1}[\beta_1 |3d_{xy}\rangle + (1-\beta_1^2)^{1/2} |4p_z\rangle + \sigma |4s\rangle + b_{1x} |4p_x\rangle + b_{1y} |4p_y\rangle]$$

with $N_{B_1} = (1+\sigma^2+b_{1x}^2+b_{1y}^2)^{1/2}$

$N_{A_1} = (1+\gamma^2+\delta^2+\gamma^2\delta^2+a_{1x}^2+a_{1y}^2)^{1/2}$

$N_{B_2} = (1+b_{2s}^2)^{1/2}$

and $N_{B_3} = (1+b_{3s}^2)^{1/2}$

We now express $\Gamma(1)$ as a sum of Γ_z, as it is in Table I, plus Γ_{Ad} due to the admixed orbital. The irrep of the admixed orbital can be easily determined from Eq. (32),

$$(\Gamma_z+\Gamma_{\mathrm{Ad}})\times\Gamma_x\times(\Gamma_z+\Gamma_{\mathrm{Ad}}) = \Gamma_x + (\Gamma_y\times\Gamma_{\mathrm{Ad}}) \ . \qquad (32a)$$

The last line in (32a), and Table II(b) show that for C_{13} to be nonzero requires admixing into the ground state an orbital that transforms as the Γ_y irrep, such as $|p_y\rangle$, resulting in a nonzero ground-state electric dipole moment. Admixing $|p_y\rangle$ to the ground state allows all the terms of Eq. (24) to contribute to C_{13}. Similarly, nonzero C_{23} requires admixing $|p_x\rangle$. Note also that admixture of $|4s\rangle$ to the ground state will make C_{33} nonzero.

In Table III we show quantitatively how the coefficients C_{13}, C_{23}, and C_{33} depend upon the admixing coefficients, defined in Table IV, of the HAOM states. These three LEFE coefficients are the only ones that contribute at the low-field endpoint. Throughout Table III the $|B\rangle$ state orbital hybridization parameters β_1, β_2, and β_3 are in the range 0.80 to 0.94, which makes the lower $|B\rangle$ states predominantly of $3d$ character and the higher $|B'\rangle$ states mainly of extended $4p$ character. We also use $\delta=1.0$ to allow the two $|A_1\rangle$ states to have both $|3d_{z^2}\rangle$ and $|3d_{x^2-y^2}\rangle$ components. In Table III, cases A and B, $1a-1d$, reflect the proof in the above paragraph that breaking the D_2 symmetry by adding $|p_y\rangle$ to the ground state will produce nonzero C_{13}, and likewise for $|p_x\rangle$ and C_{23}.

Adding $|p_x\rangle$ and $|p_y\rangle$ to the ground state produces nonzero LEFE coefficients consistent with the azurin and stellacyanin experimental data of Peisach and Mims.[12] However, the HAOM must now be reorthonormalized in order for the treatment to give valid quantitative calculations. Before doing that, we will show that breaking the D_2 symmetry of the HAOM by modifying the $|A_1\rangle$ state is an alternative way to produce C_{13} and C_{23}.

D. Modification of $|A_1\rangle$ to produce $\sigma_{\perp,3}$

One can determine by inspection which orbital should be admixed into the $|A_1\rangle$ state of the HAOM of Table I in order to produce a nonzero $\sigma_{\perp,3}$. L_z connects $|3d_{x^2-y^2}\rangle$ of the A_1 excited states with $|3d_{xy}\rangle$ of the B_1 ground state, and the term from Eq. (24) that can, potentially, give a large LEFE contribution is

$$C_{i3} \sim \langle 1|L_z|m\rangle\langle m|r_i|q\rangle\langle q|L_z|1\rangle \ , \qquad (33)$$

with $|m\rangle = |q\rangle = |A_1\rangle$. However the pure D_2 $|A_1\rangle$ state would give $\langle A_1|r_i|A_1\rangle = 0$. It is this excited-state dipole moment matrix element that requires D_2-breaking orbital admixing into $|A_1\rangle$. To ascertain the irrep Γ_{Ad} of the orbital that should be mixed into $|A_1\rangle$, one again requires that the product of the irreps contain Γ_1. We find that if $\Gamma_{\mathrm{Ad}}=\Gamma_x$ (e.g., $|p_x\rangle$), then the matrix element and C_{13} will be nonzero for $\Gamma(r_i)=\Gamma_x$. Likewise, an admixture of $|p_y\rangle$ will produce nonzero C_{23}, and $|p_z\rangle$ nonzero C_{33}.

In Table III, cases A and B, $2a-2c$, show how C_{13} and C_{23} depend upon the admixing of $|p_x\rangle$ and $|p_y\rangle$ into $|A_1\rangle$ of Table I. As with admixing of $|p_x\rangle$ and $|p_y\rangle$ into the ground state, quantitative calculations require reorthogonalization of the manifold. We now treat this reorthogonalization and demonstrate how one can begin to account quantitatively for the experimental data from the blue cupric proteins, on the effect of an applied electric field on g values, in terms of HAOM models with the D_2 symmetry selectively lowered, as just described.

VI. QUANTITATIVE COMPARISON WITH EXPERIMENTAL DATA

A. Magnitude of calculated C_{i3} in relation to experimental $\sigma_{\perp,3}$

In Sec. V a general treatment was given for modeling the g-value LEFE, valid for any low-symmetry cupric site, based upon modifications of a D_2 HAOM. We showed explicitly how group theory can be used to determine easily the symmetry properties required of admixed orbitals in order to simulate various LEFE signals, and will now focus specifically on the low-symmetry cupric site in azurin.

In order to explore the potential of g-value perturbation alone to account for the observed signal, it is con-

venient to define the quantity

$$C_{\perp,3} \equiv \left[\frac{C_{13}^2 + C_{23}^2}{2} \right]^{1/2} \tag{34}$$

and then to arrive at $C_{\perp,3}^{\max}$, the magnitude of $C_{\perp,3}$ which would be required if it were entirely responsible for the experimental value of $\sigma_{\perp,3}$. The LEFE data for azurin have $\sigma_{\perp,3} = 0.73 \times 10^{-9}$ cm/V.[12] This value is divided by 8.06×10^{-5} to get σ in units of Å/cm^{-1}, units in which it is convenient to calculate the C_{ij} from Eq. (24). Applying Eq. (11), with $g_3 = 2.27$ for azurin, one finds

$$RC_{\perp,3}^{\max} = 2.1 \times 10^{-5} \text{ Å/cm}^{-1} . \tag{35}$$

As discussed in the Appendix, at the present time we will take for the ratio R the Lorentz factor $(2+\epsilon_i)/3$, where ϵ_i is the dielectric constant of ice. At the low temperatures used in the experiment $\epsilon \sim 3$ (Ref. 29), which makes $R \sim \frac{5}{3}$. Therefore $C_{\perp,3}$, from Eq. (34) into which the C_{ij} calculated from Eq. (24) are entered, should be compared with

$$C_{\perp,3}^{\max} = \frac{2.1 \times 10^{-5} \text{ Å/cm}^{-1}}{R} = 1.3 \times 10^{-5} \text{ Å/cm}^{-1} . \tag{35a}$$

Also, for azurin, $|C_{33}| = 0.52 \times 10^{-5}$ Å/cm^{-1}.

B. Reorthonormalization of manifold with ground-state modifications

To make quantitative calculations based upon the admixtures of Sec. V requires reorthonormalization of the HAOM manifold. The renormalization of individual states is of course trivial, but reorthogonalization involves several states simultaneously and presents various options. If $|p_x\rangle$ and $|p_y\rangle$ are added, the ground state must be reorthogonalized with respect to the $|B_2\rangle$ and $|B_3\rangle$ excited states. (Rigorously, the ground state should also be reorthogonalized with respect to the $|B_2'\rangle$ and $|B_3'\rangle$ excited states. However, inclusion of these states would make reorthogonalization significantly more complicated with a small effect on the results, and will therefore not be included at this time.) By inspection of the states in Table I, we can see that if $|p_y\rangle$ is added to the ground state, orthogonalization could be accomplished by adding either $|d_{xy}\rangle$ or $|p_z\rangle$ to the $|B_2\rangle$ state. Instead, we add $|4s\rangle$ to both the ground state and the $|B_2\rangle$ and $|B_3\rangle$ states.

There are two reasons for using $|4s\rangle$ to reorthogonalize the states. First, introducing $|4s\rangle$ into the ground state has already been determined to be of great use in simulating the observed azurin hyperfine data[16] and therefore has a separate justification outside of the LEFE simulation. Second, adding $|p_x\rangle$ or $|p_y\rangle$ into the ground state implies the presence of a residual ligand electric field along the molecular x or y axes. These same electric fields have the correct symmetry properties to admix $|4s\rangle$ into the $|B_2\rangle$ and $|B_3\rangle$ excited states, thus making the admixtures self-consistent in terms of the ligand fields.

The admixings of $|4s\rangle$, $|p_x\rangle$, and $|p_y\rangle$ into the ground state, $|p_x\rangle$ and $|p_y\rangle$ into the $|A_1\rangle$ state, and $|4s\rangle$ into the $|B_2\rangle$ and $|B_3\rangle$ states are represented in the HAOM model of Table IV, in which we have included only those states from Table I that are directly involved in the calculation of C_{13} and C_{23}.

Using the states of Table IV, we attempt to quantify the experimental LEFE data on azurin by determining what admixing coefficients will lead to calculated C_{13} and C_{23} values as required by Eqs. (34) and (35a). It is informative either to let b_{1x} and b_{1y} (taken equal, as will a_{1x} and a_{1y}, for simplicity) be nonzero or a_{1x} and a_{1y} be nonzero, in order to separate the effects of D_2-breaking admixing into the ground state from admixing into the $|A_1\rangle$ state. The coefficients β_1, β_2, β_3, γ, δ are, of course, present when the site is taken to have D_2 symmetry. In order to reduce the dimension of the coefficient search space, we constrain the β coefficients and σ (the admixing coefficient of $|4s\rangle$ into the ground state—not to be confused with $\sigma_{\perp,3}$ which characterizes the experimental LEFE data) to values that have been found realistic in simulating various spectral data from low-symmetry cupric sites in proteins.[16,18] The additional requirement of orthogonality of the states then couples the ground-state admixing coefficients to the excited-state admixing coefficients and the number of undetermined parameters available to simulate the LEFE data is reduced to 1.

Cases A and B, lines 3, of Table III show the effects upon C_{i3} of varying b_{1x} (and consequently b_{1y}, b_{2s}, and b_{3s}) with σ of the ground state kept constant. As can be seen in lines 3b and 3c, to produce a value of $C_{\perp,3}$ near $C_{\perp,3}^{\max}$ of Eq. (35a) requires moderate mixing of D_2-breaking orbitals into the ground state (4–8%) and a larger D_2-breaking admixture into excited states $|B_2\rangle$ and $|B_3\rangle$. Lines 4a and 4b (together with lines 3a) show that, at constant b_{1x}, reduction in σ increases $C_{\perp,3}$; stated differently, by decreasing σ one can obtain $C_{\perp,3}$ of appropriate size with smaller admixtures to the ground state. Relatively large values of $C_{\perp,3}$ can be generated with moderate x and y character in the ground state, e.g., case B4c.

C. Reorthonormalization of manifold with $|A_1\rangle$ state modification

In Sec. V it was shown that C_{13} and C_{23} will be nonzero if the D_2 symmetry of the HAOM is broken by adding $|p_x\rangle$ and $|p_y\rangle$ into the $|A_1\rangle$ state. To quantify the size of the admixing coefficients requires reorthonormalization of the manifold involved. The mixing of $|p_x\rangle$ and $|p_y\rangle$ into $|A_1\rangle$ forces modification of the $|B_2\rangle$ and $|B_3\rangle$ states and again we introduce $|4s\rangle$ into these states to effect orthogonalization. Orthogonalization also requires $|4s\rangle$ to be present in the $|A_1\rangle$ state. This is easily justified by the fact that $|4s\rangle$ transforms as the Γ_1 irrep of the D_2 point group and could be present in $|A_1\rangle$ before the symmetry is lowered, as shown in Table I.

The requirements of orthogonality and axiality again restrict the number of free parameters introduced by the D_2-breaking admixtures. Table III shows how the C_{i3} vary with the size of $a_{1x}=a_{1y}$ (which determines the value for $b_{2s}=b_{3s}$). In cases A and B, lines 5, $\gamma=0.20$, which implies a small ($\sim 2\%$) contribution of the D_2-allowed $|4s\rangle$ in the $|A_1\rangle$ state. In cases A and B, lines 6, $\gamma=0.50$, which implies a larger $|4s\rangle$ character ($\sim 10\%$). Lines 5c show that if $\gamma=0.20$, a 2–4 % contribution from each of $|p_x\rangle$ and $|p_y\rangle$ to the $|A_1\rangle$ state will give calculated $C_{\perp,3}$ values at least $\frac{2}{3}C_{\perp,3}^{\max}$ of Eq. (35a). However, this also requires admixture of $|4s\rangle$ into both the $|B_2\rangle$ and $|B_3\rangle$ states of not less than 10%, which is rather large. Lines 6b show that if γ is raised to 0.50, then $\frac{2}{3}C_{\perp,3}^{\max}$ of Eq. (35a) can be reached again with a 2–4 % contribution from each of $|p_x\rangle$ and $|p_y\rangle$ to the $|A_1\rangle$ state, but now with only a 2–6 % admixture of $|4s\rangle$ into both the $|B_2\rangle$ and $|B_3\rangle$ states. Clearly the smaller admixtures of D_2-breaking orbitals are preferable because they imply smaller modifications of the versatile D_2 model.

VII. CONCLUSION

Within the framework of a hybrid atomic orbital model, we have investigated the linear electric field effect on the g values of low-symmetry cupric sites. Starting with D_2 symmetry electronic states based upon other experimental data (optical absorption, CD, EPR, MCD), we have used group-theoretic selection rules to determine symmetry-breaking modifications necessary to account for observed LEFE signals. Admixture of $|p_x\rangle$ and $|p_y\rangle$ orbitals to the ground or $|A_1\rangle$ excited states, along with the admixture of $|4s\rangle$ to the $|B_2\rangle$ and $|B_3\rangle$ states, leads to LEFE signals calculated from g-value perturbation which account in large part for the data from blue cupric proteins.

There is another contribution to the LEFE signal not discussed in this paper. The presence of an applied electric field will also have an effect on hyperfine interactions due to the perturbation of the orbitals. This is not the modulation of the spin-echo envelope that has been studied earlier[26] but a hyperfine effect that can produce a dc shift in the size of the observed LEFE signal. The potential importance of this hyperfine contribution is that, through reducing the magnitude required of the calculated C_{ij}, it may lead to good quantitative agreement with the data from blue cupric proteins with relatively small values of the D_2-breaking admixture coefficients, including a value for σ close to that used in simulations of EPR hyperfine splittings. A realistic HAOM would be able to reproduce data from a variety of measurements with the same coefficients. Small symmetry-breaking admixtures are attractive because they leave the model close to belonging to the well-understood, readily visualized, point group D_2. Our preliminary investigation of hyperfine effects on the LEFE indicates that they add to the g-value signal calculated here and allow the use of reasonably small D_2-breaking admixtures, including a value of σ in the range determined from other experiments. We report on this in a future paper.

ACKNOWLEDGMENT

The support of the National Science Foundation under Grant No. DMB-8517819 is acknowledged with appreciation.

APPENDIX: LOCAL ELECTRIC FIELD

The experimental $\sigma_{\perp,3}$ are given in terms of the mean fractional shift in g per unit *applied* electric field $\mathbf{E}_{\text{applied}}$, but the calculated C_{i3} depend upon the *local* electric field $\mathbf{E}_L$ actually experienced by the paramagnetic site. As indicated in Sec. II D, the equations that connect the C_{i3} and $\sigma_{\perp,3}$ should have the former multiplied by the factor

$$R=E_L/E_{\text{applied}} . \tag{A1}$$

This relation, between the local and applied electric fields, is considered below. The approach employed here in calculating R is based upon the Lorentz cavity field approximation.[27] If the cupric ion were part of a homogeneous crystal of dielectric constant ϵ, this approach would give $E_L=E_{\text{applied}}(\epsilon+2)/3$, resulting in $R=(\epsilon+2)/3$. In the case at hand, the cupric ion is in a more complicated environment.

We picture the cupric ion as located in a protein shell that can be viewed as a continuous medium of dielectric constant $\epsilon_p(T)$, which is surrounded by the continuous medium of ice with a dielectric constant $\epsilon_i(T)$. This picture faces the same complication found in Lorentz field treatments, namely, how to handle corrections due to the nearest and next-nearest neighbors of the ion of interest. The Lorentz treatment separates the local electric field into contributions from several sources. If the volume occupied by the protein molecule were assumed to be a spherical vacuum, then the electric field within that volume would be

$$E_0^p=E_{\text{applied}}\frac{\epsilon_i+2}{3} . \tag{A2}$$

The approximation of the protein as spherical is not bad for the case of azurin which has been described as a "flattened pear,"[28] and has both prolate and oblate characteristics. However, the copper atom, while not exposed to the solvent, is located near the surface rather than in the central region of the molecule. Figure 1(a) shows the general features of the system consisting of the copper atom bound within the protein structure which is, in turn, surrounded by the ice phase. One can begin to quantify the factors influencing the local electric field by taking the system to have spherical symmetry, i.e., the copper atom is at the center of a spherical shell of protein. The local electric field experienced by the cupric site is now split into separate contributions:

$$E_L^{\text{Cu}}=E_0^p+E_1^p+E_2^p+E_3^p . \tag{A3}$$

E_0^p is the field produced by all charges external to the protein molecule, Eq. (A2). E_1^p is the depolarization field from the surface charge induced on the protein molecule when it acquires an induced dipole moment. E_2^p is the Lorentz cavity field, the field from induced charges on the inside surface of an imaginary spherical cavity within

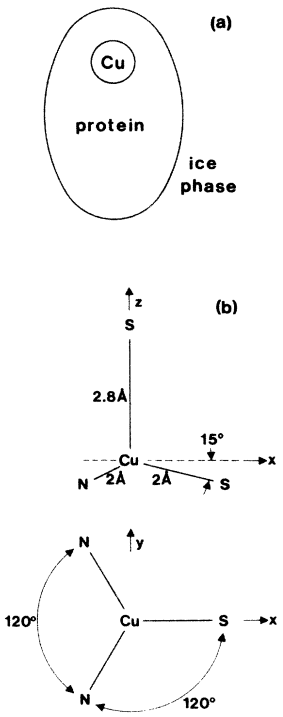

FIG. 1. (a) Schematic view of blue cupric protein molecule in frozen solution. (b) Idealized site geometry. The sulfur atom lying above the copper atom is not shown in the lower drawing.

the protein and concentric with the Cu site. The cavity is normally pictured large enough to include nearest and next-nearest neighbors. E_3^p is the field from charges or dipoles inside the cavity.

The overall average electric field in the protein is

$$E^p = E_0^p + E_1^p = E_0^p/\epsilon_p \ . \tag{A4}$$

If the protein is assumed spherical then $E_1^p = -P^p/3\epsilon_p$ where P^p is the volume polarization of the sample.[27] This gives an average electric field in the protein of

$$E^p = E_0^p + E_1^p = E_0^p/\epsilon_p = E_0^p - P^p/3\epsilon_p \ . \tag{A4a}$$

To find the local electric field at the cupric site, assumed to be at the center of a spherical cavity inside the protein, we must add E_2^p. If the cavity is spherical and the polarization is uniform in the continuous medium surrounding the cavity, then the electric field E_2^p at the center of the cavity due to the surface charge density on the inner surface of the cavity is[27]

$$E_2^p = P^p/3\epsilon_p \ . \tag{A5}$$

Adding up all the contributions to the local field (but ignoring E_3^p for the moment) gives

$$E_L^{\mathrm{Cu}} = E_0^p + E_1^p + E_2^p = E_0^p - P^p/3\epsilon_p + P^p/3\epsilon_p$$
$$= E_0^p = E_{\mathrm{applied}}(\epsilon_i + 2)/3 \ . \tag{A6}$$

Equation (A6) shows that the local electric field experienced by the cupric site does not depend on the presence of the protein shell. This is only true if the protein molecule and the imaginary cavity centered within it are spherical, in which case the electric field of the induced polarization charges on the outer surface of the protein, E_1^p, cancels with the electric field of the induced charges on the inner surface, E_2^p. If the shape of the protein is not spherical like the imaginary cavity, then E_1^p and E_2^p will not completely cancel. Furthermore, the surface of the protein is not uniform, there being hydrophobic patches in azurin (and plastocyanin). The structure of the water immediately surrounding the proteins of interest is not accurately known at this time.

Contributions to the local field from the nearest neighbors, E_3^p of Eq. (A3), will have an effect. Part of this effect is incorporated in calculations employing the HAOM, a model which implicitly includes covalency, but there are other sources to be considered. In the blue cupric proteins, at the present stages of refinement of x-ray-determined structures, the copper atom is seen to be roughly coplanar with, and bonded to, three atoms at distances of 2.0–2.2 Å (a thiolate sulfur and two imidozole nitrogens); the copper is also bonded to a thioether sulfur about 3 Å distant.[29] By considering the idealized model of this site shown in Fig. 1(b), one can estimate the magnitude and anisotropy of the contribution to E_3^p from electric dipoles induced in the atoms. Here, the radius of the Lorentz cavity is 2.8 Å with the copper atom at the center; at 2 Å are one sulfur and two nitrogens, and also included in the cavity at 2.8 Å is the second sulfur. The values of polarizability are taken as 1 and 3 Å^3 for N and S, respectively.[30] One can readily calculate that an electric field in the x direction (parallel to the copper-thiolate sulfur bond) is increased by 50% at the copper atom. In the y and z directions, the field is decreased by 25%. These numbers serve to demonstrate that electric dipoles induced inside the Lorentz cavity probably have a significant effect upon the local field. The approach of water molecules to the cupric site must also be considered. While the hydrophobic environment of the site, shown in crystallographic models,[28,29] would repel water molecules, a nonrandom arrangement of nearby waters could, possibly, produce a noticeable electric field at the copper atom. Without detailed information on where these water molecules are located, there is little upon which to base a calculation, even to the extent of determining the sign of their contribution to E_3^p. For the present, then, we take the effect of E_3^p to be negligible, in which case Eq. (A6) applies and leads to the result that the R of Eq. (A1) is the usual Lorentz factor $R = (\epsilon_i + 2)/3$. $\epsilon_i \simeq 3$ at liquid-nitrogen temperature and below,[31] so $R \simeq \frac{5}{3}$.

[1]G. W. Ludwig and H. H. Woodbury, Phys. Rev. Lett. **7**, 240 (1961).
[2]N. Bloembergen, Science **133**, 1363 (1961).
[3]W. B. Mims, Phys. Rev. **140**, A531 (1965).
[4]A. Kiel, Phys. Rev. **148**, 247 (1966).
[5]A. Kiel and W. B. Mims, Phys. Rev. **153**, 378 (1967).
[6]C. A. Bates, J. Phys. C **1**, 877 (1968).
[7]A. B. Roitsin, Usp. Fiz. Nauk **105**, 677 (1971) [Sov. Phys.—Usp. **14**, 766 (1971)].
[8]W. B. Mims, *The Linear Electric Field Effect in Paramagnetic Resonance* (Clarendon, Oxford, 1976).
[9]J. Peisach and W. B. Mims, Proc. Nat. Acad. Sci. **70**, 2979 (1973).
[10]W. B. Mims and J. Peisach, Biochem. **13**, 3346 (1974).
[11]W. B. Mims and J. Peisach, J. Chem. Phys. **64**, 1074 (1976).
[12]J. Peisach and W. B. Mims, Eur. J. Biochem. **84**, 207 (1978).
[13]R. Malkin and B. G. Malmstrom, Adv. Enzymol. **33**, 177 (1970).
[14]J. Peisach and W. E. Blumberg, Arch. Biochem. Biophys. **165**, 691 (1974).
[15]A. S. Brill and G. F. Bryce, J. Chem. Phys. **48**, 4398 (1968).
[16]A. S. Brill, *Transition Metals in Biochemistry* (Springer, Berlin, 1977).
[17]A. S. Brill, R. B. Martin, and R. J. P. Williams, in *Electronic Aspects of Biochemistry,* edited by B. Pullman (Academic, New York, 1964), p. 519.
[18]B. S. Gerstman and A. S. Brill, J. Chem. Phys. **82**, 1212 (1985).
[19]W. B. Mims, Phys. Rev. **133**, A835 (1964).
[20]W. B. Mims, Rev. Sci. Instrum., **45**, 1583 (1974).
[21]L. D. Landau and E. M. Lifshitz, *Quantum Mechanics* (Pergamon, London, 1958).
[22]J. H. Van Vleck, *Theory of Electric and Magnetic Susceptibilities* (Oxford University Press, New York, 1932).
[23]C. S. Smith, in *Solid State Physics,* edited by F. Seitz and D. Turnbull (Academic, New York, 1958), Vol. 6, p. 175.
[24]M. Tinkham, *Group Theory and Quantum Mechanics* (McGraw-Hill, New York, 1964).
[25]J. Peisach and W. B. Mims, Chem. Phys. Lett. **37**, 2, 307 (1976).
[26]L. G. Rowan, E. L. Hahn, and W. B. Mims, Phys. Rev. **137**, A61 (1965); W. E. Blumberg, W. B. Mims, and D. Zuckerman, Rev. Sci. Instrum. **44**, 546 (1973).
[27]C. Kittel, *Introduction to Solid State Physics,* 5th ed. (Wiley, New York, 1976).
[28]E. T. Adman, R. E. Stenkamp, L. C. Sieker, and L. H. Jensen, J. Mol. Biol. **123**, 35 (1978).
[29]G. E. Norris, B. F. Anderson, and E. N. Baker, J. Mol. Biol. **165**, 501 (1983).
[30]C. H. Rhee, R. M. Metzger, and F. M. Wiygul, J. Chem. Phys. **77**, 899 (1982).
[31]*Physics and Chemistry of Ice Symposium,* edited by E. Whalley (Royal Society of Canada, Ottawa, 1972).